Spectral element FNPF simulation of focused wave groups impacting a fixed FPSO

Engsig-Karup, Allan P.; Eskilsson, Claes

Published in:
Proceedings of the 28th International Ocean and Polar Engineering Conference — 2018

Publication date:
2018

Document Version
Publisher's PDF, also known as Version of record

Proceedings of the Twenty-eighth (2018) International Ocean and Polar Engineering Conference
Sapporo, Japan, June 10-15, 2018

ISBN 978-1-880653-87-6; ISSN 1098-6189

www.isope.org

Spectral Element FNPF Simulation of Focused Wave Groups Impacting a Fixed FPSO

Allan P. Engsig-Karup
Department of Applied Mathematics and Computer Science
Center for Energy Resources Engineering (CERE)
Technical University of Denmark
Kongens Lyngby, Denmark

Claes Eskilsson
Research Institutes of Sweden (RISE)
Borås, Sweden
Department of Civil Engineering
Aalborg University
Aalborg Ø, Denmark

ABSTRACT

For the assessment of experimental measurements of focused wave groups impacting a surface-piecing fixed structure, we present a new Fully Nonlinear Potential Flow (FNPF) model for simulation of unsteady water waves. The FNPF model is discretized in three spatial dimensions (3D) using high-order prismatic - possibly curvilinear - elements using a spectral element method (SEM) that has support for adaptive unstructured meshes. This SEM-FNPF model is based on an Eulerian formulation and deviates from past works in that a direct discretization of the Laplace problem is used making it straightforward to handle accurately floating structural bodies of arbitrary shape. Our objectives are; i) present detail of a new SEM modelling developments and ii) to consider its application to address a wave-body interaction problem for nonlinear design waves and their interaction with a model-scale fixed Floating Production, Storage and Offloading vessel (FPSO). We first reproduce experimental measurements for focused design waves that represent a probably extreme wave event for a sea state represented by a wave spectrum and seek to reproduce these measurements in a numerical wave tank. The validated input signal based on measurements is then generated in a NWT setup that includes the FPSO and differences in the signal caused by nonlinear diffraction is reported.

KEY WORDS: Spectral element method; high order numerical methods; unstructured meshes; fully nonlinear potential flow; focused wave; wave-body interaction; FPSO.

INTRODUCTION

Significant efforts have been made for several decades to develop reliable tools based on fully nonlinear potential flow theory that can handle real geometries of offshore structures and bodies, cf. Karimirad, Michailides & Nematbakhsh (2018). The most mature developments for industrial applications in coastal engineering and offshore engineering are of Boussinesq-type addressing the wave propagation problem, cf. Brochini (2013), however, these models can conventionally only handle the fluid-structure interaction problem for simple structures and bodies due to the depth-integrated assumption used in the derivation procedures. Even today, handling both the wave propagation problem and the wave-body interaction problem is challenging and is most often considered by hybrid modelling approaches where two different simulation tools are combined through weak coupling.

To resolve these restrictions within a single numerical model, we focus on a complete modelling approach in the setting of potential flow that offer much more flexibility in the numerical discretization procedure. In this work, we propose a SEM-FNPF model, that can handle both the wave propagation problem and the wave-body interaction problem using a multi-element spectral element model that has support for adaptive unstructured meshes with curvilinear elements to represent arbitrarily shaped bodies. The model relies on the recent progress made in two spatial dimensions for a stabilized spectral element method for an Eulerian free surface flow model by Engsig-Karup, Eskilsson & Bigoni (2016) for the wave propagation problem, and Engsig-Karup, Montesering & Eskilsson (2018) on the stabilization of a Mixed Eulerian-Lagrangian (MEL) formulation. A recent description of state-of-the-art for spectral element methods are given in Hui, Cantwell, Monteserin, Eskilsson, Engsig-Karup and Sherwin (2018). In this work, we present the new spectral element method in 3D based on an Eulerian formulation. We discard the σ-transformation that was used in Engsig-Karup & Eskilsson (2016). To introduce a surface-piercing fixed body inside the fluid domain, we solve the Laplace problem and discretize this model equation directly and discretize using curvilinear high-order elements based on transfinite interpolation for the free surface layer of elements.

WAVE BASSIN EXPERIMENTS

The experiments we seek to reproduce in this work was conducted as a part of the FROTH project carried out at Plymouth University in the COAST Laboratory facility in UK. In the experiments a fixed scale-model of a FPSO is considered and it is subjected to focused design wave events that are designed to be probable extreme events taken from an irregular sea state based on JONSWAP spectrums. The FPSO has a fixed position with a draft of 0.153 m in still water, a box length of 0.9

m from the centers of the semicircular bow and stern. The radii of the semicircular parts are 0.15 m resulting in a total length of FPSO of 1.2 m (Model 3). The FPSO hull has vertical sides. The still water depth (h) in the part of the basin that contains the FPSO is 2.93 m and is the part that is considered in our numerical wave tank experiments.

The purpose of the experiments was to assess factors such as wave steepness and wave run-up on FPSO hulls due to extreme wave events. We consider Part 1 of these experiments where waves of different steepness and angle of incidence are considered. We consider the incident angle of 0 degree only (Part I experiments) in this paper and compare the numerical results to the measured results obtained using an array of resistive wave gauges. Only access to partial results for the measurements with no FPSO in the basin have been provided as a part of the blind test experiment among different simulation tools. This work provides details of a new solver we have designed and proposed in connection with this blind test experiment and represent a contribution that is a result of our ongoing effort to produce new and improved numerical tools for nonlinear wave propagation and wave-body interactions. Excellent numerical results for same experimental campaign have been produced using the QALE-FEM model is reported by Ma, Yan, Greaves, Mai & Raby (2015).

GOVERNING EQUATIONS

The governing equations for FNPF equations is expressed in the form of the Eulerian formulation expressed in terms of free surface only variables, cf. derivation in Engsig-Karup, Glimberg, Nielsen & Lindberg (2013). Let the fluid domain $\Omega \in \mathbb{R}^d$ be a bounded, connected domain with a piece-wise smooth boundary $\Gamma \in \mathbb{R}^{d-1}$. Let $T : t \geq 0$ be the time domain. We seek a scalar velocity potential function $\phi(x,z,t) : \Omega \times T \to \mathbb{R}$ satisfying the Laplace problem

$$\begin{aligned} \phi &= \tilde{\phi}, \quad \text{on} \quad \Gamma^{FS} \\ \nabla^2\phi &= 0, \quad \text{in} \quad \Omega \\ \nabla\phi \cdot \nabla h &= 0, \quad \text{on} \quad \Gamma^b \end{aligned} \tag{1}$$

Where $h(x) : \Gamma^b \to \mathbb{R}$ describes the still water depth, however, that is assumed constant in this work. The temporal evolution of the water surface is described by $z = \eta(x,t) : \Gamma^{FS} \times T \to \mathbb{R}$. The notations are illustrated in Fig. 1. The unsteady free surface kinematic and dynamic boundary conditions are expressed in the Zakharov (1968) form

$$\begin{aligned} \partial_t\eta &= -\boldsymbol{\nabla}\eta \cdot \boldsymbol{\nabla}\tilde{\phi} + \tilde{w}(1 + \boldsymbol{\nabla}\eta \cdot \boldsymbol{\nabla}\eta) \quad \text{in} \quad \Gamma^{\mathrm{FS}} \times T, \\ \partial_t\tilde{\phi} &= -g\eta - \frac{1}{2}\left(\boldsymbol{\nabla}\tilde{\phi} \cdot \boldsymbol{\nabla}\tilde{\phi} - \tilde{w}^2(1 + \boldsymbol{\nabla}\eta \cdot \boldsymbol{\nabla}\eta)\right) \quad \text{in} \quad \Gamma^{\mathrm{FS}} \times T, \end{aligned} \tag{2}$$

where we in the free surface equations eq. (2) have assumed the gradient definition $\nabla = (\partial_x, \partial_y)$, '$\sim$' is used to denote free surface variables defined at $z = \eta$, and g is the gravitational acceleration defined to be 9.81 m/s^2. We note that the free surface equations have been expressed in terms of free surface variables only.

To determine the wave-induced pressures at a fixed body, we can use Bernoulli's equation

$$\frac{p}{\rho} = -gz - \phi_t - \frac{1}{2}\nabla\phi \cdot \nabla\phi, \tag{3}$$

which require the evaluation of ϕ_t. The density of the fluid is represented by ρ . Following the approach of Tanizawa (1995) which is used in the work of Monteserin, Engsig-Karup & Eskilsson (2018) in connection with their proposed spectral element method we determine ϕ_t using the acceleration potential method. The pressures can be integrated to estimate forces on the structures, however, is not reported in this paper, since the aim is to compare to a few experimental measurement records for surface elevation only due to limited space.

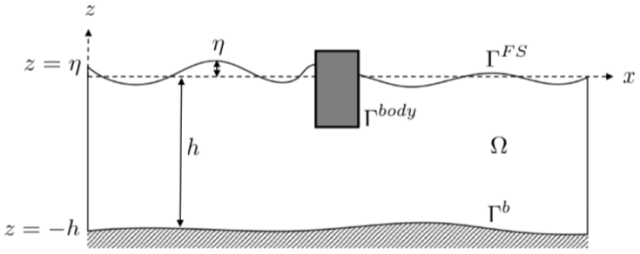

Figure 1. Notations used to describe the numerical model and numerical discretization.

WAVE GENERATION AND ABSORPTION

To generate waves in a wave maker zone and absorb waves in a sponge layer zone, we use the embedded penalty forcing technique that takes the form

$$\partial_t f = \mathcal{N}_f(x,t) + (1 - \gamma(x))\tau^{-1}(f_a(x,t) - f(x,t)), \quad (x,t) \in \Gamma^{FS} \times T \tag{4}$$

where $\mathcal{N}_f(x,t)$ is the nonlinear right hand side functions of the semi-discrete system of equations eq. (2) where $f = \eta, \tilde{\phi}$, the relaxation functions $0 \leq \gamma(x) \leq 1$ defined following Engsig-Karup (2006), and the source function $f_a(x,t)$ defines the analytical representation of the wave input signal. The parameter τ is chosen equal to the time step size Δt.

NUMERICAL DISCRETIZATION

The numerical discretization procedure for the Eulerian formulation described in Engsig-Karup, Eskilsson & Bigoni (2016) is followed for the free surface problem, however, is changed for the Laplace problem by discarding the σ-transformation.

We form a partition of the domain to obtain a tessellation $\mathcal{T}_h$ consisting of N_{el} non-overlapping regular elements $\mathcal{T}_h^k$ such that $\mathcal{T}_h^k \subset \mathcal{T}_h$ with k denoting the k'th element. We introduce the finite element approximation space of continuous, piece-wise polynomial functions of degree at most P

$$V = \{v_h \in C^0(\Gamma_h^{FS}); \forall k \in \{1, ..., N_{el}\}, v_{h|\mathcal{T}_k} \in \mathbb{P}^P\} \tag{5}$$

The weak formulation of the free surface equations takes the form. Find $f \in V$ where $f = \eta, \tilde{\phi}$ such that

$$\begin{aligned} \iint_{\Gamma^{\mathrm{FS}}} \partial_t\eta v(\boldsymbol{x})d\boldsymbol{x} &= \iint_{\Gamma^{\mathrm{FS}}} [-\boldsymbol{\nabla}\eta \cdot \boldsymbol{\nabla}\tilde{\phi} + \tilde{w}(1 + \boldsymbol{\nabla}\eta \cdot \boldsymbol{\nabla}\eta)]v(\boldsymbol{x})d\boldsymbol{x} \\ \iint_{\Gamma^{\mathrm{FS}}} \partial_t\tilde{\phi} v(\boldsymbol{x})d\boldsymbol{x} &= \iint_{\Gamma^{\mathrm{FS}}} \left[-g\eta - \frac{1}{2}\left(\boldsymbol{\nabla}\tilde{\phi} \cdot \boldsymbol{\nabla}\tilde{\phi} - \tilde{w}^2(1 + \boldsymbol{\nabla}\eta \cdot \boldsymbol{\nabla}\eta)\right)\right] v(\boldsymbol{x})d\boldsymbol{x} \end{aligned} \tag{6}$$

For all $v \in V$. We introduce the finite-dimensional approximations

$$f_h(\boldsymbol{x},t) = \sum_{i=1}^{N^{FS}} f_i(t)N_i(\boldsymbol{x}), \tag{7}$$

Where $\{N_i\}_{i=1}^{N_{FS}} \in V$ is the set of global finite element functions with cardinal property $N_i(\mathbf{x_j}) = \delta_{ij}$ at mesh nodes with δ_{ij} the Kronecker symbol. Substitute eq. (7) and the choice of test functions into eq. (6)

where we choose $v(\boldsymbol{x}) \in \{N_i\}_i^{N_{FS}}$ for Galerkin discretization. The discretization in two spatial dimensions becomes

$$M' \frac{d}{dt}\eta_h = -\left(A_x^{\tilde{\phi}_x} + A_y^{\tilde{\phi}_y}\right)\eta_h + M'\tilde{w}_h + \left(A_x^{\tilde{w}_h(\eta_h)_x} + A_y^{\tilde{w}_h(\eta_h)_y}\right)\eta_h$$
$$M' \frac{d}{dt}\tilde{\phi}_h = -M' g\eta_h - \frac{1}{2}\left[\left(A_x^{(\tilde{\phi}_h)_x} + A_y^{(\tilde{\phi}_h)_y}\right)\tilde{\phi}_h + M^{\tilde{w}_h}\tilde{w}_h - \left(A_x^{\tilde{w}_h^2(\eta_h)_x} + A_y^{\tilde{w}_h^2(\eta_h)_y}\right)\right]\eta_h \quad (8)$$

where the following global matrices have been introduced

$$M'_{ij} = \iint_{\Gamma^{FS}} N_i N_j d\boldsymbol{x}, \;\; M^b_{ij} = \iint_{\Gamma^{FS}} b(\boldsymbol{x}) N_i N_j d\boldsymbol{x}, \;\; (A^b_q)_{ij} = \iint_{\Gamma^{FS}} b(\boldsymbol{x}) N_i \frac{\partial}{\partial q} N_j d\boldsymbol{x}. \quad (9)$$

All elemental integrals are subject to a change of variable from the physical element into a reference element via the affine mapping $\chi^k : \mathcal{T}_h^k \mapsto \mathcal{T}_r$ where $\mathcal{T}_r$ is the reference prism element described in the next section. The gradients of the free surface state variables are recovered using global L^2 Galerkin projection. Temporal integration of the semi-discrete equation system given in eq. (8) is performed using an explicit fourth-order Runge-Kutta method. Exact integration of the interpolating polynomial representations of the integrands is used for the evaluation of the integrals to avoid quadrature errors in the inner products of the discrete weak form of the free surface equations in line with Engsig-Karup, Eskilsson & Bigoni (2016). A non-expensive conforming 2D mild spectral filter designed to be used for free surface variables in line with this previous work in 2D and with the simulation of Peregrine breathers in 3D considered by Koukounas, Eskilsson & Engsig-Karup (2018). In this work, the spectral filter is constructed to filter off 5% of the top mode of the hierarchical modal expansion and 1% of the second highest polynomial modes. The filter is active every time step of the simulation and does not affect mass conservation and has minor effect on the energy of the wave propagation.

The spatial discretization of the Laplace equation is based on discarding the σ-transformation that was used in the previous work of Engsig-Karup, Eskilsson and Bigoni (2016). Thereby, we avoid the unnecessary complication of a time-dependent σ-transformation when handling nonlinear waves and floating bodies, e.g. see Cai, Langtangen, Nielsen & Tveito (1998) that used a penalty scheme to account for a submerged cylindrical body in a σ-transformed 2D FEM model. Our view is that such approaches are difficult to generalize to handle submerged or surface-piercing bodies due to the σ-transformation in the setting of nonlinear wave-body problems. However, the price for more geometric flexibility is the need for a dynamic mesh-update procedure that may increase the computational cost due to the need for updating the mesh every time step.

We consider the weak formulation of the Laplace problem

$$\int_{\mathcal{T}_h} \nabla\cdot\nabla\phi v dx = \oint_{\partial\mathcal{T}_h} v\mathbf{n}\cdot\nabla\phi dx - \int_{\mathcal{T}_h} \nabla\phi\cdot\nabla v dz = 0, \quad (10)$$

For all $v \in V$ where the boundary integrals vanish at domain boundaries where impermeable structural boundaries are assumed for the walls of the numerical wave tank as well as the fixed FPSO body considered in this work. The discretization of the last term in eq. (10) leads to discrete coefficient matrix that is defined via domain decomposition as

$$\mathcal{L}_{ij} = -\int_{\mathcal{T}_h} (\nabla N_j)\cdot(\nabla N_i) dx = -\sum_{k=1}^{N_{el}^{2D}} \int_{\mathcal{T}_h^k} (\nabla N_j)\cdot(\nabla N_i) dx. \quad (11)$$

All elemental integrals are subject to a change of variable from the physical element into a reference element via the affine mapping $\chi^k : \mathcal{T}_h^k \mapsto \mathcal{T}_p$ where $\mathcal{T}_p$ is the reference prism element described in the next section. Thus, the numerical discretization leads to a sparse linear symmetric system of equations

$$\mathcal{L}\phi_h = \mathbf{b}, \quad \mathcal{L} \in \mathbb{R}^{n\times n}, \quad \mathbf{b} \in \mathbb{R}^n, \quad (12)$$

where n is the total degrees of freedom in the discretization. This linear system is modified to impose the dirichlet boundary conditions at the free surface such that

$$\mathcal{L}_{ij} = \delta_{ij}, \quad \mathbf{b}_i = \tilde{\phi}_i, \quad \boldsymbol{x}_i \in \Gamma^{FS}. \quad (13)$$

The gradients of the globally piece-wise continuous basis functions are recovered using global L^2 Galerkin projection that takes the general and compact form, e.g. for $f_h = u_h, v_h, w_h$

$$\int_\Omega f_h v dx = \int_\Omega (f_h)_X v dx \quad (14)$$

where $X = x, y, z$ leading to the corresponding linear system of equations

$$M f_h = S_X \phi_h \,. \quad (15)$$

To recover the coefficients f_h of the expansion described by eq. (7) we can solve eq. (15) to recover the gradient variable values at mesh nodes.

MESH ELEMENTS

The fluid domain is decomposed into prism elements in the time-constant computational domain. The prism elements are formed by triangulating the horizontal plane with an unstructured two-dimensional mesh generator. Each of the resulting triangular elements can then be extended (extrude operation) in the vertical from the surface to the bottom. A spectrally accurate multivariate hierarchical polynomial expansion for a reference prism element (see Karniadakis & Sherwin (2005)) can be constructed by collapsing the coordinates of the cube

$$\mathcal{Q} = \{(r,s,t) \in \mathbb{R}^3 : -1 < r,s,t < 1\}\,, \quad (16)$$

into a prism through the transformation

$$x = r, \quad y = \tfrac{1}{2}(1+s)(1-r) - 1, \quad z = t. \quad (17)$$

Skipping the *t*-coordinate the triangular reference element used at the free surface is defined as

$$\mathcal{T}_r = \{(r,s) \in \mathbb{R}^2 : -1 < r,s < 1; r+s < 0\}, \quad (18)$$

and the prism element assumes coordinates in a reference element

$$\mathcal{T}_p = \{(r,s,t) \in \mathbb{R}^3 : -1 < r,s,t < 1; r+s < 0; t < 1\}. \quad (19)$$

We introduce the element hierarchical basis functions associated with this transformation in the form for prism elements

$$\tilde{\varphi}_{\mathbf{k}}(\mathbf{r}) = \tilde{P}_{k_1}^{(2k_2+1,0)}(r)\tilde{P}_{k_2}^{(0,0)}(s)(1-s)^{k_2}\tilde{P}_{k_3}^{(0,0)}(t)\,, \quad (20)$$

where $\tilde{P}_n^{(\alpha,\beta)}(\xi)$ is the n'th order orthonormal Jacobi polynomial on the interval $\xi \in [-1,1]$ with orthogonality property

$$\int_{-1}^{1} \tilde{P}_m^{(\alpha,\beta)}(\xi)\tilde{P}_n^{(\alpha,\beta)}(\xi)(1-\xi)^\alpha(1+\xi)^\beta d\xi = \delta_{mn}, \;\; \tilde{P}_n^{(\alpha,\beta)} = \frac{P_n^{(\alpha,\beta)}}{||P_n^{(\alpha,\beta)}||_{L^2_w([-1,1])}}. \quad (21)$$

These polynomials can efficiently be generated and evaluated using a

simple recurrence relation for Jacobi polynomials, cf. Hesthaven, Gottlieb & Gottlieb (2007). The modal basis for prism element eq. (20) have a mixed polynomial order $k_1 + k_2$ in the horizontal plane and polynomial order k_3 in the vertical. The basis for triangular elements is obtained by omitting the vertical polynomial dependence. The model is implemented to be able to tune the orders of the approximations to balance accuracy and efficiency needs for concrete applications. The curvilinear elements that are used to represent the semi-circular parts of the FPSO hull are parametrized as described in Canuto, Hussaini, Quarteroni & Zang (2006). The prism elements that share a top face with the free surface use a curvilinear representation for this face and the inner nodes are adjusted using transfinite interpolation in the vertical coordinate before mapping to the reference element used for discretization.

MESH GENERATION

We employ GMSH due to Geuzaine & Remacle (2009) for mesh generation by defining the numerical wave tank and taking into account the surface of the FPSO in a 2D layer defined at the bottom of the FPSO. This 2D mesh surface is extruded to the still water level while accounting for the FPSO body. Another layer is obtained by extruding to the bathymetry to the $z = -h(x)$. In this way, two prismatic layers are obtained, one that captures the FPSO geometry and one layer below the FPSO. The physical wave tank has dimensions 35.5 m long with a width of 15.5 m. We setup the numerical wave tank with a reduced to size 12 m times 8 m, with a wave maker of size 1.63 m (distance from left boundary to WG1) in first part of the domain and a long sponge layer of 10.40 m in the last part that can effectively dampen all the harmonics of the wave group. The volumetric mesh for the NWT with the FPSO hull is illustrated in Fig. 2.

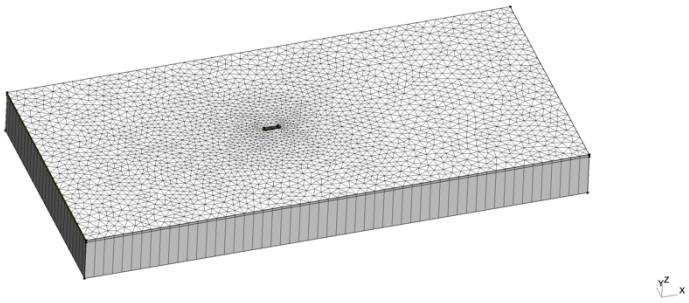

Figure 2. Illustration of an unstructured mesh for the Numerical Wave Tank with the FPSO representation. The mesh generated consists of two vertical layers of prismatic elements inside the numerical wave tank. A thin upper layer has thickness corresponding to the draft of the FPSO. This layer includes a representation of the FPSO surface.

The mesh consists of 12440 prism elements and hereof 6208 triangular elements in the free surface layer. The mesh is adjusted ad hoc in the SEM solver where the FPSO surface is automatically detected and the semi-circular front and back of the FPSO is represented using curvilinear prismatic elements in the upper layer, cf. Fig. 3. The computations reported in this paper are all based on using elements with polynomial orders $P_h = 5$ in horizontal directions and $P_v = 3$ in the vertical direction. This resolution has been chosen to balance accuracy and efficiency needs to deliver the results presented for the submission.

DESIGN FOCUSED WAVE GROUP

A focused wave group is in the original experiment determined using New Wave theory due to Tromans, Anatürk & Hagameijer (1991) and is based on a JONSWAP spectrum with parameters (CCP-WSI ID 13BT1) A= 0.09363 m, Tp = 1.362 s, h = 2.93 m, Hs = 0.103 m, kA = 0.21. Out of the Part I experiments this corresponds to the most nonlinear wave group.

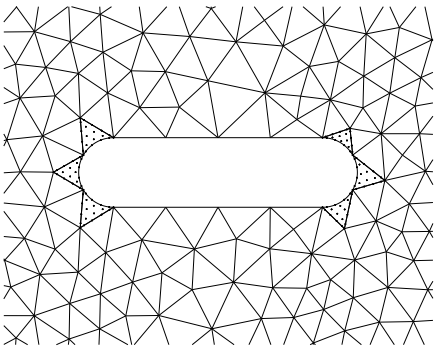

Figure 3. Top-view illustration of the unstructured mesh in upper layer with a few curvilinear iso-parametric prism elements of polynomial order $P_h = 5$ at the semi-circular bow and stern of the FPSO.

In this work, we choose the path to reverse engineer the experimental setup by relying on the signal measured in the original experiment and reconstructed using a Fourier analysis. This helps reduce the size of the domain to not waste computational resources, and to reproduce the experiments as close as possible, since the exact wave signal generation procedure for the paddle software is not known in detail. We take the time series of the free surface elevation measured at WG1 and perform a FFT analysis to decompose the signal for the free surface elevation into a truncated Fourier representation using *N* modes matching the number of measurements in the time series. From the complex coefficients of the FFT series representation, we extract the estimated amplitude a_n and phase ϵ_n of each harmonic in the series. We verify that the signal is reproduced correctly by comparing against the measured time series. Then, for each harmonic in the series, we solve the dispersion relation

$$k_n h = \sqrt{\frac{\omega_n^2}{g} k_n h^2 \coth(k_n h)} \tag{22}$$

iteratively to obtain the wave number k_n of harmonic mode *n* given the still water depth and angular frequency to estimate the phase speed $c_n = \omega_n / k_n$ matching the depth. We keep the modes with wave numbers k_n<200 to keep only the *M* most important longest harmonic components and reduce total number of terms (*M*<*N*) in the series representation for quicker evaluations. These modes are still higher resolution than the modes that can be resolved in the wave signal represented in the numerical SEM solver, such that it is numerical truncation errors that dominates the errors. The numerical resolution should be sufficient to resolve free waves of *kh*<15 to within an estimated 2% error in linear dispersion error, cf. Fig. 5b in Engsig-Karup, Eskilsson & Bigoni (2016). A snapshot of the generated focused wave group is seen in Fig. 4. The input wave signal is constructed as a linear superposition of the exact linearized regular traveling waves in the form for mode *n* in the truncated series representation

$$\begin{aligned} \eta_n(x,t) &= a_n \cos(\omega_n t - k_n x + \epsilon_n) \\ \phi_n(x,t) &= -a_n c_n \frac{\cosh(k_n h)}{\sinh(k_n h)} \sin(\omega_n t - k_n x + \epsilon_n) \end{aligned} \tag{23}$$

The input wave signal is generated in a wave maker zone that begin at the western domain boundary of the NWT and end at the position of WG1. The input wave signal is generated in this wave maker zone

through superposition of the truncated Fourier series accounting for the phase speed of each component and phase in the measured signal to reproduce approximately the signal at WG1. The generated wave group propagate freely from the position of WG1 that is at the interface to the computational domain to interact with the FPSO hull. The wave group is designed to focus at the bow position of the FPSO hull.

Figure 4. Snapshot of a generated focused wave group inside a numerical wave tank used for input signal validation.

NUMERICAL RESULTS

The New Wave input signal described in former section is generated in a wave generation zone and propagated to the location of the FPSO. To validate the setup, the wave is compared to the analytical at the point target for focusing. First, we carry out a validation case, where we consider the generation of the input wave signal in a wave tank with no FPSO. The wave gauge layout for the experiments are illustrated in Fig. 5. A time step size of $\Delta t = 0.025$ s is used in all simulations. In Fig. 6 we show the generated signals at the position of WG1 in the NWT with and without the FPSO hull. These results confirm that signal for the free surface elevation is reproduced correctly. We compare the simulated wave heights with the measurement of selected WG's in Fig. 7 for the Reference setup. The results for the reference setup confirm that our setup is in good agreement with the experimental setup in the physical wave basin, and that most of the time series measurements are reproduced with good accuracy. However, the signal peaks are under predicted suggesting that the wave group is under resolved due to lack of spatial resolution to capture dispersion correctly for the shortest harmonics. This will be investigated in more detail for the conference.

In a new experiment, we generate the same wave input signal in the wave maker zone and extract the measurement according to the layout described here when the FPSO is positioned in the NWT. Clearly the signal now differs at some WGs, cf. Fig 8 and compare to Fig. 7. Especially the WG24 signal has changed due to the presence of the FPSO in NWT the that leads to shadowing of the wave group and wave scattering of waves away from the hull during the impact of the wave group. The objective is to contribute with refined results to the blind test experiment Part I of the Collaborative Computational Project in Wave Structure Interaction (CCP-WSI) initiative (https://www.ccp-wsi.ac.uk/) for a comparison among several wave simulation tools at ISOPE 2018.

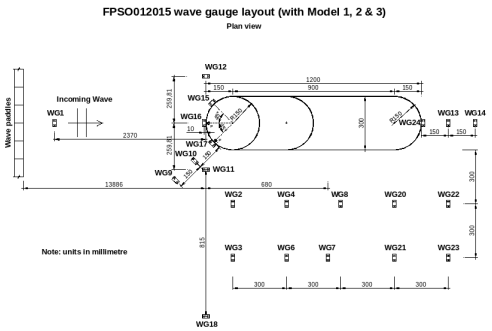

Figure 5. Experimental layout of wave gauges in the FROTH project.

We report here the results for the free surface run-up on the hull of the FPSO and surface elevations. The measurements reported here are taken at positions at the bow of the FPSO using WG16 and WG17, the stern of the FPSO using WG24, and in the vicinity of the FPSO using WG7. In Fig. 7, we compare the reference measurements for a NWT without the FPSO. In Fig 8, we compare the computed results with the reference measurements to highlight differences that result from the presence of the FPSO and leads to wave scattering caused by diffraction of the nonlinear waves interacting with the hull that influence the propagating focused wave group.

We highlight that the stabilised SEM-FNPF model presented here represents a new solver approach that can be seen as an efficient alternative to much more computationally expensive CFD simulators based on Navier-Stokes equations in line with the review given in Ma & Yan (2009). The proof-of-concept simulations presented have been run on a CPU using sequential but vectorized code for Matlab v17a with CPU timings up to 4.5 days. We have highlighted how the proposed SEM-FNPF modelling approach is well suited for wave propagation simulation that interacts with arbitrarily shaped bodies where breaking does not occur.

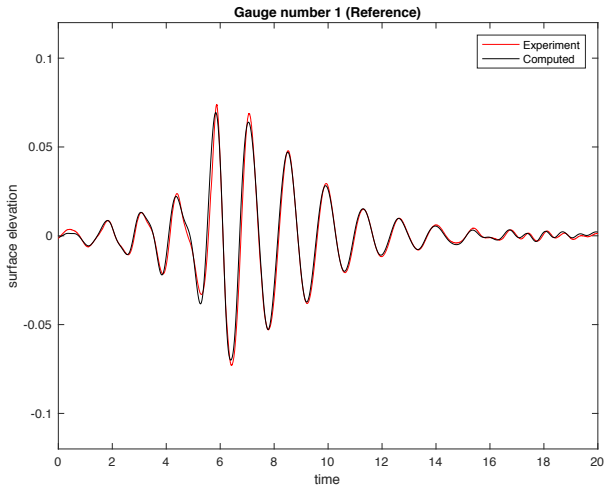

Figure 6. Wave gauge 1 (WG1) measurements comparison for NWT with FPSO. WG1 is the measurement signal (Experiment) reproduced in the wave maker zone. The time is started at t=38s of the measurement signal and corresponds to t=0s in the computed results.

CONCLUSIONS

We have proposed a new spectral element model SEM-FNPF for the spatial discretization of FNPF equations. Through direct discretization of the Laplace equation together with the introduction of curvilinear elements in the free surface elements, it is possible handle nonlinear wave-body interactions. This approach gives the necessary flexibility to describe fixed (and moving bodies), however requires adaptive mesh updates that may add additional cost to the numerical efficiency over σ-transformed modelling approach. We have considered the case of a fixed surface-piercing body in the form of a FPSO hull and compared to reference measurements for focused wave groups generated from an irregular series that defines a focused wave group from a random sea state. The comparison of the numerical results in the reference setup, show excellent agreement with the input signal generated as expected, and also good agreement with the wave gauge measurements positioned later in the numerical wave tank. Due to the linear superposition of harmonics obtained from the FFT analysis, we expect some errors in the wave maker zone not accounted for in the analysis as

a result of the nonlinear wave propagation. The computed results for the setup where a FPSO is present, shows that the wave scattering changes the signals, which is most pronounced at the stern of the FPSO.

In ongoing work, the proposed new SEM-FNPF model will be prepared for handling also freely moving structures of relevance for applications in marine renewable energy and prepared for large-scale simulations using high-performance computing.

ACKNOWLEDGEMENTS

This work contributes to the activities in the research project Multi-fidelity Decision making tools for Wave Energy Systems (MIDWEST) that is supported by the OCEAN-ERANET program. The DTU Computing Center (DCC) has supported the work with access to computing resources. Claes Eskilsson is partially supported by the Swedish Energy Agency through grant no 41125-1.

REFERENCES

Brocchini, M. (2013). "A reasoned overview on Boussinesq-type models: the interplay between physics, mathematics and numerics". *Proc. Roy. Soc. London Ser. A, 469* (2160), pp. 1–27.

C. Canuto, M.Y. Hussaini, A. Quarteroni, T.A. Zang, Spectral Methods - Fundamentals in Single Domains, Springer, 2006.

Cai, X., Langtangen, H.P., Nielsen, B.F. and Tveito, A. 1998. "A finite element method for fully nonlinear water waves", *J. Comput. Phys*. 143, 544-568.

Engsig-Karup A.P. (2006) "Unstructured nodal DG-FEM solution of high-order Boussinesq-type equations", Ph.D. thesis, in series: (ISBN: 87-89502-63-9), pages: 214, Technical University of Denmark.

Engsig-Karup, A. P., Glimberg, L. S., Nielsen, A. S. and Lindberg, O. 2013. Fast hydrodynamics on heterogeneous many-core hardware. Part of: Raph¨ael Couturier. Designing Scientific Applications on GPUs (ISBN: 978-1-4665-7162-4), pages 251–294, 2013, CRC Press / Taylor & Francis Group.

Engsig-Karup, A.P., Eskilsson C. and Bigoni, D. (2016) "A Stabilised Nodal Specral Element Method for Fully Nonlinear Water Waves", J. *Comput. Phys.,* 318, pp. 1-21.

Engsig-Karup, A.P. Eskilsson, C. and Bigoni, D. (2016) "Unstructured Spectral Element Model for Dispersive and Nonlinear Wave Propagation", The International Society of Offshore and Polar Engineers (ISOPE), Rhodos, Greece.

Geuzaine, C. and Remacle, J.-F. (2009) Gmsh: A 3-D finite element mesh generator with built-in pre- and post-processing facilities, Sep 10, 2009.

Hesthaven, J.S., Gottlieb, S. and Gottlieb, D. Spectral Methods for Time-Dependent Problems, Cambridge Monographs on Applied and Computational Mathematics, vol. 21, Cambridge University Press, Cambridge, UK, 2007.

Karimirad, M., Michailides, C. and Nematbakhsh, A. (2018) "Numerical Methods in Offshore Fluid Mechanics". In book: Offshore Mechanics: Structural and Fluid Dynamics for Recent Applications.

Karniadakis, G.E., Sherwin, S.J. (2005) Spectral/*hp* Element Methods for Computational Fluid Dynamics, 2nd edition, Oxford University Press.

Koukounas, D., Eskilsson, C. & Engsig-Karup, A.P. (2018) "Numerical simulations of Peregrine breathers using a spectral element model", Proceedings of the ASME 2018 37th International Conference on Ocean, Offshore and Artic Engineering (OMAE), June, Madrid, Spain.

Ma, Q.W. and Yan, S. (2009). "QALE-FEM for numerical modelling of non-linear interaction between 3D moored floating bodies and steep waves", International Journal for Numerical Methods in Engineering, 78, 713-756.

Ma, Q., Yan, S., Greaves, D., Mai, T., Raby, A., (2015) "Numerical and Experimental Studies of Interaction between FPSO and Focusing Waves", in Proceedings of 25th ISOPE conference, 21-26 June, Hawaii, USA, Vol.3: 655-662.

Monteserin, C., Engsig-Karup, A.P. and Eskilsson, C. (2018) "Nonlinear Wave-body Interaction using a Mixed-Eulerian-Lagrangian Spectral Element Model", Proceedings of the ASME 2018 37th International Conference on Ocean, Offshore and Artic Engineering (OMAE), June, Madrid, Spain.

Tanizawa, K., (1995) "A nonlinear simulation method of 3-D body motions in waves", *Jap. Soc. of Naval Arch*.,178(1), pp. 179–191.

Tromans P.S., Anatürk A. R., Hagameijer P. (1991) "A new model for kinematics of large ocean waves - Application as a design wave." Proc. First Int. Offshore and Polar Engng. Conf., pp 64 – 71, Edinburgh, UK.

Xui, H., Cantwell,, C.D., Monteserin, C, Eskilsson, C., Engsig-Karup, A.P., and Sherwin, S. J. Spectral/*hp* element methods: Recent developments, applications, and perspectives, Journal of Hydrodynamics, February 2018, Volume 30, Issue 1, pp. 1-22.

Zakharov, V.E. (1968) "Stability of periodic waves of finite amplitude on the surface of a deep fluid", *J. Appl. Mech. Tech. Phys*. 9, pp. 190–194.

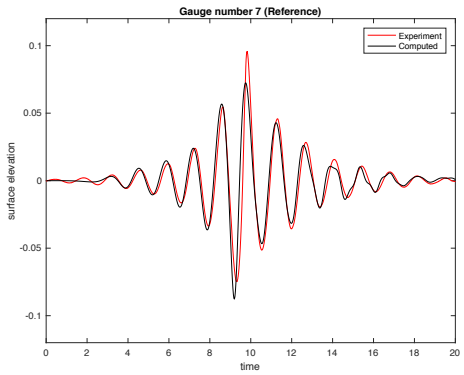

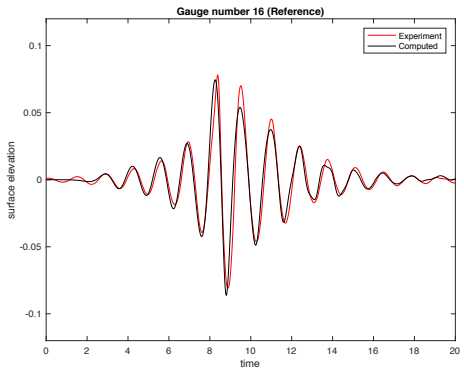

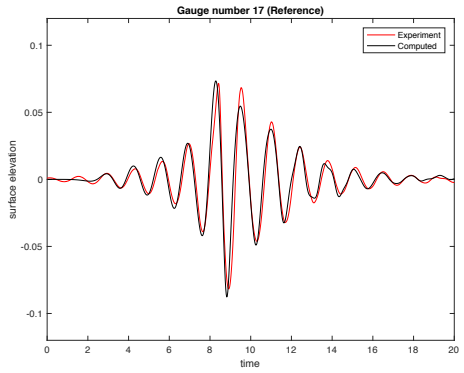

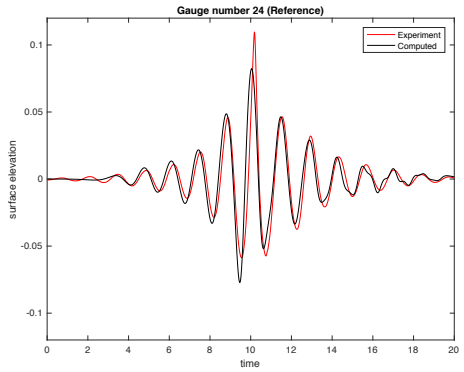

Figure 7. Wave Gauge measurements comparison for NWT in reference setup (without FPSO). The time is started at t=38s of the measurement signal and corresponds to t=0s in the figures.

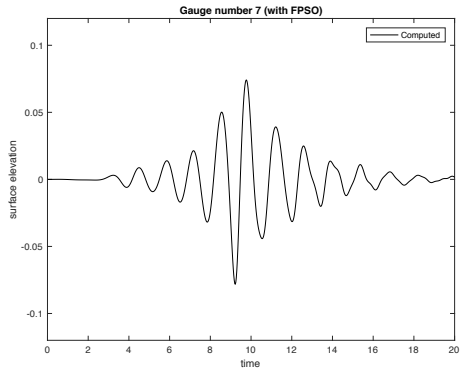

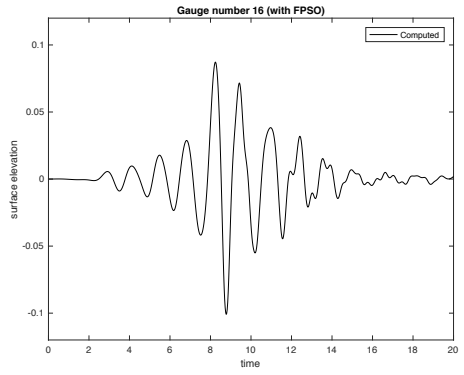

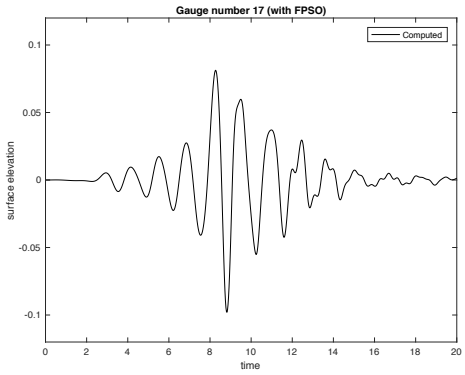

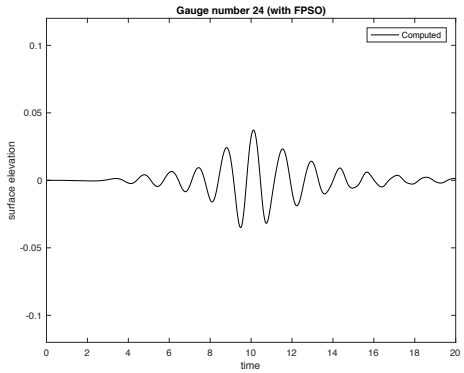

Figure 8. Compute Wave Gauge measurements for NWT with FPSO. The time is started at t=38s of the measurement signal and corresponds to t=0s in the figures.

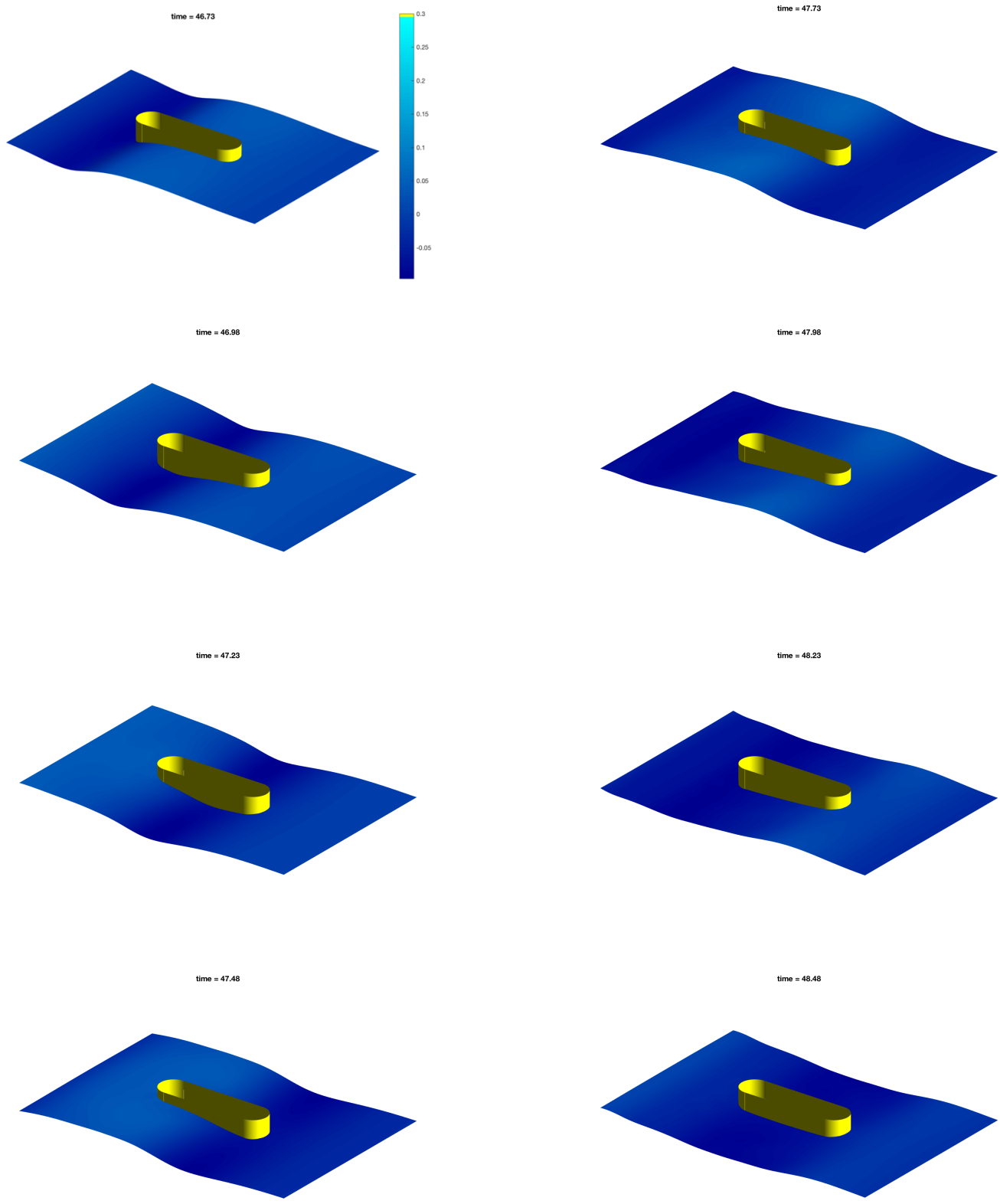

Figure 9. Snapshots of the free surface in vicinity of the FPSO hull. The impacting wave group is propagating from left to right along the FPSO hull. The indicated times match those of the original experiments. The scale is 1:1 matching the experimental setup.